remote sensing

MDPI

Article

Persistent Urban Park Cooling Effects in Krakow: A Satellite-Based Analysis of Land Surface Temperature Patterns (1990–2018)

Ewa Głowienka * and Marcin Kucza

Department of Photogrammetry, Remote Sensing, and Spatial Engineering, Faculty of Geo-Data Science, Geodesy, and Environmental Engineering, AGH University of Krakow, 30-059 Krakow, Poland; mkucza@agh.edu.pl
* Correspondence: eglo@agh.edu.pl; Tel.: +48-8820-29813

Highlights

What are the main findings?

- Multi-decadal Landsat analysis shows persistent park cooling.
- Vegetation moisture drives stronger cooling than greenness.

What are the implications of the main findings?

- Urban parks act as long-term heat mitigation assets.
- Water management in green spaces boosts cooling benefits.

Abstract

Urban green spaces provide measurable cooling that can mitigate urban heat islands, yet few studies have quantified these effects over multiple decades. This study analyzed Landsat imagery from four epochs (1990, 2000, 2013, 2018) to derive land surface temperature (LST) and vegetation indices—NDVI for greenness and NDMI for moisture content—for four large urban parks in Krakow. Late spring/summer LST in parks was compared with that of urban areas within 0–150 m and 150–300 m of park boundaries. Statistical significance was evaluated using bootstrapped confidence intervals, long-term trends were assessed via the Mann–Kendall test, and correlation analysis was used to examine relationships between LST and each vegetation index. Results show a persistent park cooling effect, with park interiors ~2–3 °C cooler than adjacent urban areas in all years. Despite an overall city-wide LST rise of ~5–6 °C from 1990 to 2018, the park cool island intensity (temperature difference between park and city) remained stable (no significant long-term trend, $p > 0.7$). Bootstrapped 95% confidence intervals confirmed that each park's cooling effect was statistically significant in each year analyzed. NDMI (vegetation moisture content) correlated more strongly with LST ($r \sim -0.90$) than NDVI ($r \sim -0.7$ to -0.9), highlighting the importance of vegetation moisture in park cooling. These findings demonstrate that well-watered urban parks can sustain substantial cooling benefits over decades of urban development. The persistent ~2–3 °C daytime cooling observed underscores the value of water-sensitive green space planning as a long-term urban heat mitigation strategy.

Keywords: park cool island (PCI); land surface temperature (LST); Landsat; NDVI; NDMI

check for updates

Academic Editor: Christopher Small

Received: 11 September 2025
Revised: 22 October 2025
Accepted: 28 October 2025
Published: 31 October 2025

Citation: Głowienka, E.; Kucza, M. Persistent Urban Park Cooling Effects in Krakow: A Satellite-Based Analysis of Land Surface Temperature Patterns (1990–2018). *Remote Sens.* **2025**, *17*, 3608. https://doi.org/10.3390/rs17213608

Copyright: © 2025 by the authors. Licensee MDPI, Basel, Switzerland. This article is an open access article distributed under the terms and conditions of the Creative Commons Attribution (CC BY) license (https://creativecommons.org/licenses/by/4.0/).

1. Introduction

Urbanization and climate change are intensifying the urban heat island (UHI) effect—cities tend to be warmer than their rural surroundings, especially at night and during

heatwaves, leading to increased heat stress and cooling energy demand [1,2]. Globally, rapid urban development has been linked to significant rises in land surface temperatures and loss of vegetated areas in recent decades [3,4]. Thermal remote sensing provides a valuable means to monitor urban temperature patterns over time [4,5], using satellite data (e.g., Landsat, MODIS) to map LST consistently across entire cities [4–6]. This enables analysis of how urban expansion and vegetation loss contribute to surface heating [3,4]. However, a multi-decadal assessment of urban surface temperatures requires careful cross-sensor continuity and atmospheric standardization. For reflective bands, documented cross-calibration between Landsat-7 ETM+ and Landsat-8 OLI provides the basis for consistent vegetation metrics [7,8], while operational OLI/TIRS atmospheric correction and validation frameworks enable stable radiometry [9]. For thermal retrieval, generalized and revised single-channel (SC) approaches tailored to Landsat-8/9 Band 10 are widely adopted and validated [10–12]. Although several reviews have noted the rapid the growth of Surface Urban Heat Island (SUHI) research, they also emphasize that few studies exploit the full 30+ year Landsat record to track urban climate trends rather than static city–rural contrasts [5,13]. This underscores the importance of long-term analyses for capturing urban climate trajectories. Seasonal and diurnal controls are essential for such analyses: by holding phenological phase (late-spring leaf-on) and local time (near-noon overpass) constant across epochs, the structural park–city LST differences can be isolated from seasonal variability. Notably, European urban-climate efforts remain dominated by air-temperature products and modeling (e.g., high-resolution 100-city air temperature fields), underscoring the complementary value of long-term satellite LST for surface-based diagnostics [14,15]. The nearly 30-year timeframe of this study goes well beyond the scope of typical European urban climate studies (which usually span only 1–5 years), allowing the detection of long-term trends that shorter analyses would likely miss.

In strategies to mitigate urban overheating, green infrastructure plays an increasingly important role. Trees, parks, and other vegetated areas absorb solar radiation and cool their surroundings through shading and evapotranspiration [16,17]. Consequently, cities exhibit the park cool island (PCI) phenomenon—lower temperatures within parks compared to the built-up urban matrix [17,18]. The PCI effect has been documented worldwide: on average, green areas are about 1 °C cooler in daytime than their surroundings, with differences of several degrees in favorable conditions [18,19]. Numerous case studies in various climate zones report daytime LST reductions on the order of 1–5 °C due to parks, depending on local conditions [18,19]. For example, in tropical and arid cities, parks have been found ~1–3 °C cooler than adjacent urban areas [18,20], while in temperate climates the cooling can be even greater—e.g., in Wroclaw, Poland, large parks were on average 2–3 °C cooler than their built environment [21], and in Nagoya, Japan, forested parks were ~3–4 °C cooler than dense urban districts in summer [18,22]. Nocturnal cooling effects also occur, though they are smaller in terms of surface temperature. After sunset, vegetation releases heat more slowly than concrete and asphalt, leading to lower night-time air temperatures over parks. In London, a large park (Kensington Gardens) was reported to be 4–6 °C cooler at night than the surrounding city, with the cooling influence extending up to ~300 m from the park's edge [18,23]. Other studies in temperate climates have likewise found that urban parks can reduce night-time air temperatures in their immediate vicinity by a few degrees, helping to alleviate UHI impacts after dark [18,23].

The strength of the PCI depends on numerous factors. Larger parks with extensive tree cover generally produce a stronger and more persistent cooling effect than small lawns or isolated groves [17,24–26]. The presence of water bodies (ponds, rivers) can further enhance cooling through increased evaporative potential [11,17]. In contrast, small pocket parks and individual street trees provide only localized microclimate cooling [17,24]. Climate is also

an important modulator: in humid or temperate cities the cooling effect of vegetation tends to be more pronounced than in hot, arid regions [5,27,28]. Limited water availability in dry urban environments constrains plant transpiration, so vegetation has a weaker impact on surface temperature there [5,27,28].

Despite substantial progress in understanding PCIs, important knowledge gaps remain. Most remote sensing studies of urban vegetation's cooling influence have been cross-sectional—focusing on single cities or single points in time [18,19]. A recently published global study of >2000 parks across 371 cities found an average daytime cooling of ~1.5 °C (varying with park type) relative to the urban surroundings, but that study was essentially static (a one-time assessment) and did not capture changes over time [29]. This highlights the need for multi-temporal analysis of park cooling. It remains largely unknown whether and how park cooling benefits persist over multiple decades of urban growth and climate warming. A multi-decade perspective is crucial because urban landscapes and regional climates evolve over time; such an analysis can reveal whether well-designed parks continue to offset rising temperatures or whether their cooling effectiveness diminishes as urbanization intensifies and background temperatures increase. This information is critical for urban planners and climate adaptation strategies, as it indicates whether parks can serve as reliable, long-term infrastructure for mitigating urban heat.

To address this knowledge gap, the present study provides a rare long-term view of park cooling performance by analyzing nearly 30 years of satellite observations in a single city. We focus on Kraków, Poland, as a representative Central European city that has experienced significant urban expansion in recent decades along with substantial warming. Kraków lies in a temperate mid-latitude climate zone and contains diverse large green areas (including historic urban parks and extensive suburban forests), which allows examination of park cooling in different urban contexts. Notably, 2018 saw a record of roughly 100 hot days in Kraków [30,31], reflecting a surge in extreme heat events. This recent trend underscores the need to understand how the city's parks mitigate urban heat under climate change. In this four-epoch, seasonally controlled Landsat case study, it was examined (i) how land surface temperature (LST) in major parks has changed over time compared to the surrounding city, (ii) whether park cooling intensity (the LST difference between parks and the urban fabric) has shifted between 1990 and 2018, and (iii) the relative role of vegetation greenness versus moisture in modulating park cooling. The hypothesis was that large, vegetated parks provide stable cooling benefits despite overall warming, and that vegetation moisture (measured by the normalized difference moisture index, NDMI) will be a stronger predictor of cooling than greenness (NDVI). The results of the long-term analysis provide new insights into the sustained climate. The 30-year span of observations (with consistent seasonal timing across epochs) enables detection of long-term trends that could not be captured in shorter studies. These findings deepen the understanding of how green infrastructure regulates the urban climate over decades and will inform heat adaptation strategies in cities, especially in temperate regions similar to Kraków.

2. Materials and Methods

2.1. Study Area

The study was conducted in the metropolitan area of Krakow in southern Poland (population ~1.1 million) [32]. Krakow lies in the Vistula River valley at an elevation of ~200–300 m above sea level and has a temperate transitional climate with warm summers and cold winters [33]. Land cover in the region is diverse—it includes a dense urban core, industrial areas, agricultural fields, and patches of natural vegetation.

For analysis four major green areas that represent typical urban and peri-urban vegetation in Krakow were selected. These comprise two extensive forest complexes on the city outskirts—Wolski Forest (~419 ha on the western edge of Krakow) [34] and Zabierzowski Forest (a mixed forest to the northwest of the city)—as well as two large green spaces embedded in built-up areas [35]: the historic Planty Park (a ring of gardens encircling the Old Town) [36] and a riverside riparian forest in the east of the city (the Legowski Forest, ~186 ha) [37]. Each selected green space was treated as a polygon of interest for further spatial analysis. Figure 1 shows the locations of the four study sites within Krakow.

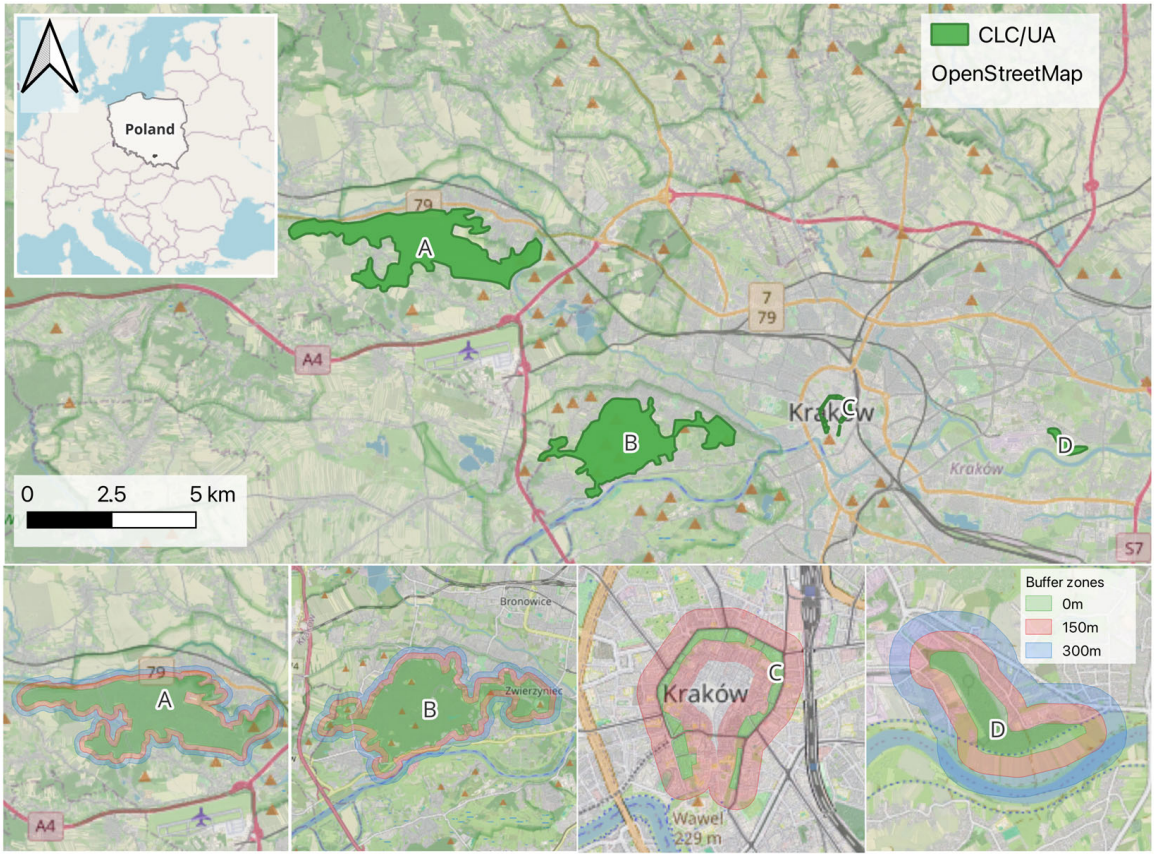

Figure 1. Four study parks in Kraków, Poland—(**A**) Wolski Forest; (**B**) Zabierzowski Forest; (**C**) Planty Park; (**D**) Legowski Forest—with analysis buffers (0 m, 0–150 m, 150–300 m). Boundaries from Urban Atlas 2018 and CLC 2018; basemap OpenStreetMap; CRS WGS 84/UTM 34N.

2.2. Data Sources and Integration

To precisely define the boundaries of the parks and buffer zones, official vector land-cover datasets from the Copernicus and European Environment Agency programs were utilized. In particular, CORINE Land Cover (CLC) data for the years 1990, 2000, 2012, and 2018, and Urban Atlas (UA) data for 2012 and 2018 were obtained. The CORINE Land Cover provides a consistent, pan-European land cover classification (Level 3, 44 classes) and a long temporal span from the 1990s, which is useful for multi-decade analyses. The Urban Atlas offers higher-detail land use information for Functional Urban Areas, including a specific class (14100) for urban green areas (parks). The use of these standardized data ensures consistent class definitions and mapping parameters, enabling replication of the methodology in other cities [38,39]. The CLC and Urban Atlas layers for the Krakow area were downloaded from the EEA/Copernicus repositories [38–41] and used them without generalization. The CLC tiles covering the Krakow region were mosaicked and dissolved by land-cover class. From the CLC data, polygons belonging to forest classes (3.1.1 deciduous forest, 3.1.2 coniferous

forest, 3.1.3 mixed forest) were extracted to represent the suburban woodland sites. The Urban Atlas 2012 and 2018 layers were used to identify urban park areas (class 14100). All vector data were reprojected to a common coordinate system (WGS 84/UTM zone 34N). Spatial data processing and integration were performed using QGIS 3.22.

Based on these layers, the final boundaries of each studied green space were defined. Two concentric urban buffer rings were delineated to characterize the near-field park–city transition: an inner buffer of 0–150 m and an outer buffer of 150–300 m beyond each park's boundary. The 0–150 m buffer represents the immediate urban adjacency, where the strongest horizontal LST gradients typically occur just outside the canopy edge. The 150–300 m buffer captures the remainder of the commonly reported park cooling footprint in the surrounding neighborhood. The choice of a 150 m buffer increment was motivated by empirical evidence that park cool islands generally only extend on the order of a few hundred meters into the urban fabric) [23,26,42]. These distances (on the order of 100–300 m) are representative of the outer bounds of meaningful park cooling under most conditions, aligning with prior reports in the literature [23,26,42]. The selected buffer widths correspond to the spatial resolution of the Landsat thermal data (~30 m). A 150 m ring spans roughly 5 Landsat pixels from the park edge, and the two rings together reach ~10 pixels outward. This scale provides a robust sample of urban pixels in each zone while limiting edge-mixing and geolocation uncertainty in the satellite imagery. Thus, the park interior ("0 m" zone) can be quantitatively contrasted with two successive urban zones that (i) capture the immediate park influence (0–150 m) and (ii) represent the outer, but still proximate, urban context (150–300 m) where cooling signals are often still observable. This buffering scheme ensures a clear differentiation between conditions inside parks and in their urban surroundings, and is consistent with the typical spatial footprint of park cool islands reported in other cities

2.3. Satellite Data and Preprocessing

Four cloud-free Landsat scenes from the USGS Landsat Collection 2, Level 2 product archives were analyzed. To ensure reliable long-term comparisons, one Landsat scene was carefully selected for each epoch (roughly every ten years) under nearly identical environmental conditions. All four scenes correspond to late spring, clear sky days (early May 1990, 2000, 2013, 2018) with acquisitions at noon (approximately 10:00–11:00 UTC). This timing captures peak daytime heating and fully flushed vegetation for each year, providing phenologically stable snapshots. The selection of these specific years was dictated by data availability (consistent Landsat path/row coverage and minimal cloud cover) and alignment with land cover datasets (e.g., CORINE 1990, 2000, 2012, and Urban Atlas 2018) to ensure consistent park boundary definitions. By using a fixed season and time of day for the study, the impact of seasonal or diurnal variability on LST was minimized, and the structural thermal contrast between parks and urban fabric was preserved.

All images are from the same Landsat path/row (WRS-2 path 188, row 25 covering Krakow): 1990-05-04, 2000-05-15, 2013-05-19, and 2018-05-01. Metadata for the scenes (acquisition date, time, Landsat ID) are listed in Table A1 (Appendix A).

From the surface reflectance imagery (bands Red, NIR, SWIR1), the NDVI (Normalized Difference Vegetation Index) [43], and NDMI (Normalized Difference Moisture Index) [44] indices were calculated for each pixel (Equations (1) and (2)).

$$NDVI = \frac{NIR - Red}{NIR + Red} \quad (1)$$

$$NDMI = \frac{NIR - SWIR1}{NIR + SWIR1} \quad (2)$$

Land surface temperature was retrieved using the standard single-channel LST approach for Landsat thermal bands with emissivity correction (Equations (3)–(5)) [10,45–50].

$$LST = \frac{T_B}{1 + \left(\frac{\lambda T_B}{c_2}\right) ln(\varepsilon)} \quad (3)$$

$$T_B = \frac{K_2}{ln\left(\frac{K_1}{L_\lambda} + 1\right)} \quad (4)$$

$$\varepsilon = 0.986 + 0.004 \cdot PV \rightarrow \text{where } PV = \left[\frac{NDVI - NDVI_{min}}{NDVI_{max} - NDVI_{min}}\right]^2 \quad (5)$$

T_B—brightness temperature
K_1, K_2—Landsat sensor-specific calibration constants
L_λ—at-sensor spectral radiance ($W \cdot m^{-2}\ sr^{-1}\ \mu m^{-1}$)
λ—effective wavelength of the thermal band
LST—land surface temperature in Kelvin
$c^2 = 1.4388 \times 10^{-2}$ m·K—Planck's second radiation constant
ε—emissivity
PV—fractional vegetation cover

The resulting LST represents land surface "skin" temperature in degrees Celsius. LST was initially computed at the thermal sensor's native resolution (120 m for TM; 100 m for TIRS) and then resampled to the 30 m grid to align with NDVI/NDMI and the buffer zones.

For each of the four green sites and three zones (interior 0 m, 0–150 m buffer, 150–300 m buffer), summary statistics of LST, NDVI, and NDMI were extracted for the years 1990, 2000, 2013, and 2018. These included the mean, standard deviation, interquartile range (Q25, Q75, IQR), minimum, and maximum across the pixels in each zone. Because the parks differ in area, both unweighted (arithmetic) means and area-weighted means were computed for city-level aggregation. In reporting city-wide results, the area-weighted averages (each park's contribution weighted by its area) are used to avoid bias from the different park sizes. The park cool island intensity is consistently defined as ΔLST = LST park—LST urban (so ΔLST values are negative when the park is cooler than its surroundings). The detailed per-park descriptive statistics are given in Table A2 (Appendix A). Satellite-data processing was conducted in the Google Earth Engine (GEE) cloud environment [51] and QGIS 3.22.

2.4. Trend and Statistical Analyses

To assess long-term trends (1990–2018) in key variables, Theil–Sen slope estimates were calculated for each time series and the non-parametric Mann–Kendall test was performed for monotonic trend significance [52–55]. Trends were evaluated for, e.g., the mean LST inside parks (0 m zone) and in the outer urban buffer (300 m zone), as well as for mean NDVI and NDMI within park interiors and buffers. The trend in the PCI intensity (ΔLST between park and urban zone) was also computed over time. Given the small number of time points (n = 4 years), these trend results were interpreted cautiously (α = 0.05 significance threshold). The Mann–Kendall test, while applied, has low power with $n < 8$, so the absence of a significant trend should be viewed in light of this limitation. In addition, to evaluate the statistical significance of the cooling effect in each year, a bootstrap technique and a sign test were applied. Bootstrap resampling (20,000 iterations) was used to construct 95% confidence intervals for the mean ΔLST in each year and zone combination. If the entire bootstrap CI for ΔLST lay below 0 °C (negative), the park was considered cooler than the city at a 95% confidence level. A two-sided sign test was also performed on the paired park vs. buffer LST values for the four parks in each year (H0: median difference = 0). Although

with only 4 pairs per year the sign test has low power, it provides a non-parametric check of whether all parks consistently showed cooling.

Lastly, the relationships between LST and the vegetation indices were examined. For each year (pooling all zones for that year), Pearson correlation coefficients (r) between LST and NDVI, and between LST and NDMI, were calculated using the set of observations consisting of each park–zone combination as a data point (n = 12 observations per year: 4 parks × 3 zones). These yearly correlations reflect how greener or wetter areas tended to have lower temperatures. To analyze the overall relationship across all years, the data for all parks, zones, and years (48 observations in total) were pooled and an ordinary least squares (OLS) regression of ΔLST versus ΔIndex was performed after centering values by year. Specifically, each year's city-wide mean LST and index values were subtracted to remove inter-annual level differences. The centered LST anomaly was then regressed against the centered NDVI anomaly (and similarly for NDMI) to estimate an average slope (°C change per unit index) using all data [56,57]. This OLS fit provides another measure of the index–temperature relationship strength. The annual correlation coefficients and the pooled regression slopes are reported, while over-interpretation of the exact slope magnitudes is avoided given the limited sample, in line with statistical best practices [56,57]. All trend and statistical analyses were carried out in R (v. 4.3.x, R Foundation for Statistical Computing) using the standard packages trend, Kendall, boot, and stats.

3. Results

3.1. Long-Term LST Patterns and Park Cooling Intensity

In all four analyzed years (1990, 2000, 2013, and 2018), the mean land surface temperature inside the studied green areas (0 m zone) was significantly lower than in the surrounding urban buffer zones. Table 1 summarizes the area-weighted mean LST (± standard deviation) for park interiors (0 m zone) and the two buffer zones. For example, on 04 May 1990 the parks' mean LST was 17.55 ± 0.15 °C, whereas the immediate 0–150 m urban buffers averaged 19.70 ± 0.38 °C and the 150–300 m buffers 19.85 ± 0.45 °C. By 2018, park interiors had risen to 22.99 °C while the 0–150 m and 150–300 m zones reached 25.07 °C and 25.58 °C, respectively. This represents an overall warming of about 5–6 °C in surface temperatures across both park and urban areas from 1990 to 2018, reflecting regional climate warming and urban heat gain.

Table 1. Average land surface temperature (LST, °C) ± standard deviation for the park interior (0 m) and buffer zones (150 m and 300 m) in Krakow for each study year. Values are area-weighted means across the four parks.

Year	0 m (Park Interior)	150 m Buffer	300 m Buffer
1990	17.55 ± 0.15 °C	19.70 ± 0.38 °C	19.85 ± 0.45 °C
2000	20.31 ± 0.33 °C	22.66 ± 0.58 °C	23.02 ± 0.64 °C
2013	22.10 ± 0.21 °C	24.00 ± 0.53 °C	24.28 ± 0.76 °C
2018	22.99 ± 0.45 °C	25.07 ± 0.79 °C	25.58 ± 0.95 °C

Despite this parallel warming, the park cool island (PCI) effect remained evident and of similar magnitude in each year. On average, park interiors were about 2–3 °C cooler than their surroundings. Specifically, the mean difference ΔLST = LSTpark − LSTurban (using the 0–150 m buffer as the urban reference) was approximately −2.16 °C in 1990 and −2.36 °C in 2000 (negative sign indicates cooler parks) (Table 2). In 2013 the PCI was slightly smaller (−1.90 °C), and in 2018 it was −2.09 °C. Using the outer 150–300 m ring as reference, ΔLST values were similarly around −2.2 °C (1990) to −2.7 °C (2000), as listed in

Table 2. Figure 2a plots the mean LST in parks vs. the outer urban zone over time, while Figure 2b visualizes the PCI intensity. In all cases the parks were cooler than the urban environment at a statistically significant level.

Table 2. Park cool island intensity (ΔLST = LST park − LST urban) for the four study years, with 95% confidence intervals from bootstrap resampling (B = 20,000). Negative values indicate that the park interior was cooler than the specified urban buffer zone.

Year	ΔLST (0–150 m) °C (95% CI)	ΔLST (150–300 m) °C (95% CI)
1990	−2.16 (−2.48, −1.70)	−2.31 (−2.73, −1.80)
2000	−2.36 (−2.94, −1.70)	−2.71 (−3.31, −1.98)
2013	−1.90 (−2.21, −1.43)	−2.18 (−2.65, −1.51)
2018	−2.09 (−2.51, −1.66)	−2.59 (−3.23, −1.95)

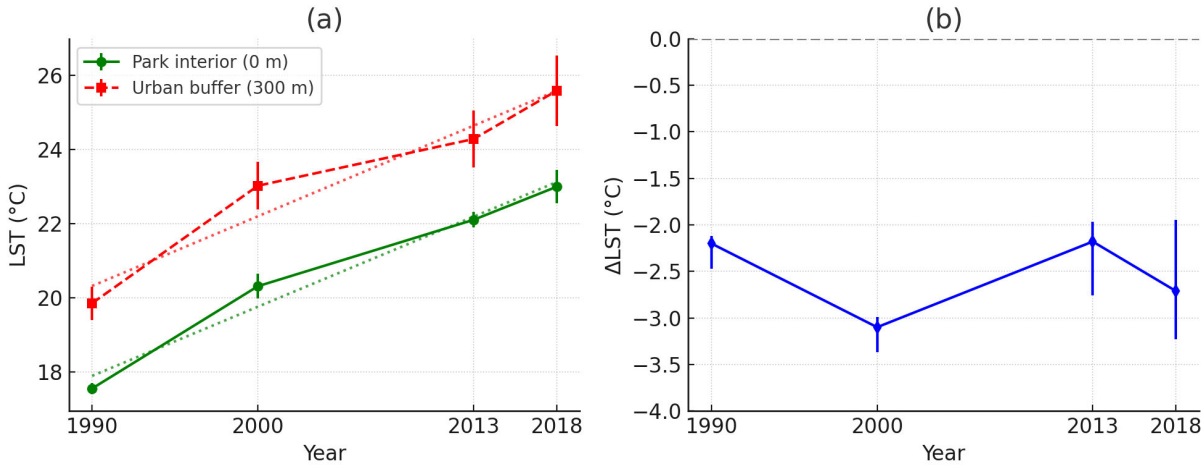

Figure 2. (**a**) Mean late spring/summer LST (°C) in park interiors (0 m) and in the outer urban buffer (300 m) for 1990–2018. Error bars show the standard deviation across the four parks. Theil–Sen trend lines are plotted (dotted), illustrating a warming trend in both zones that is not statistically significant over n = 4 years. (**b**) Park cool island intensity, ΔLST (park minus urban LST), for 1990–2018. Error bars indicate 95% bootstrap confidence intervals (B = 20,000). The cooling effect remained roughly 2–3 °C throughout the period, with no significant trend in ΔLST.

Statistical analysis confirmed the significance and consistency of these cooling differences. For each year and buffer comparison, the bootstrapped 95% confidence interval for the mean park–urban LST difference was entirely below 0 °C (Table 2). For instance, in 2018 the mean ΔLST between park interiors and the 0–300 m urban zone was −2.59 °C, with a 95% CI of [−3.23, −1.95] °C. Since this interval does not include zero, we conclude the cooling effect is significant at $\alpha = 0.05$. A non-parametric sign test further showed that all four individual parks had lower LST than their immediate urban surroundings each year (yielding $p \approx 0.125$ for n = 4 in each year, which, while not <0.05 due to the small sample, consistently indicated the same directional effect). In summary, every park in every year functioned as a cool island relative to its neighborhood.

Over the 28-year period, we detected no meaningful trend in the magnitude of the park cool island effect. The Theil–Sen estimator for the PCI (park vs. 0–150 m buffer) was a slope of +0.007 °C per year, i.e., an increase of only ~0.2 °C over 28 years, which is negligible and statistically non-significant (Mann–Kendall $\tau = 0.33$, $p = 0.75$). Using the 0–300 m comparison, the trend was even closer to zero (approximately −0.002 °C/yr). In other words, the temperature gap between parks and the city showed no sustained increase or decrease from 1990 to 2018.

The PCI magnitudes reported here are unconditional (area-weighted mean differences between zones). In the companion mixed-effects study, zone contrasts are conditional on vegetation indices and year, estimated within a linear mixed-effects framework. Consequently, the unconditional ΔLST of roughly 2–3 °C reported here appears larger than the conditional core-to-periphery contrasts of ≈1.7–2.3 °C reported there, which quantify zone effects after controlling for NDVI/NDMI and year. The two perspectives are complementary: descriptive PCI for communication and planning, and model-based PCI for effect attribution.

The cooler park interiors coincided with substantially higher vegetation index values inside the parks compared to the buffers. Distributions of NDVI and NDMI for the four years (Figures 3 and 4, respectively) show that the interior zones had consistently greater greenness and moisture than the urban surroundings. In each year, NDVI values were higher inside the parks (denoting denser, healthier vegetation) relative to the 150 m and 300 m buffers, and similarly, NDMI was highest in the park interiors and decreased with distance into the urban zone. These patterns indicate that areas with lusher, well-watered vegetation (the park interiors) corresponded to the coolest surface temperatures observed, whereas the hotter urban zones were associated with lower NDVI and NDMI (sparser or drier vegetation).

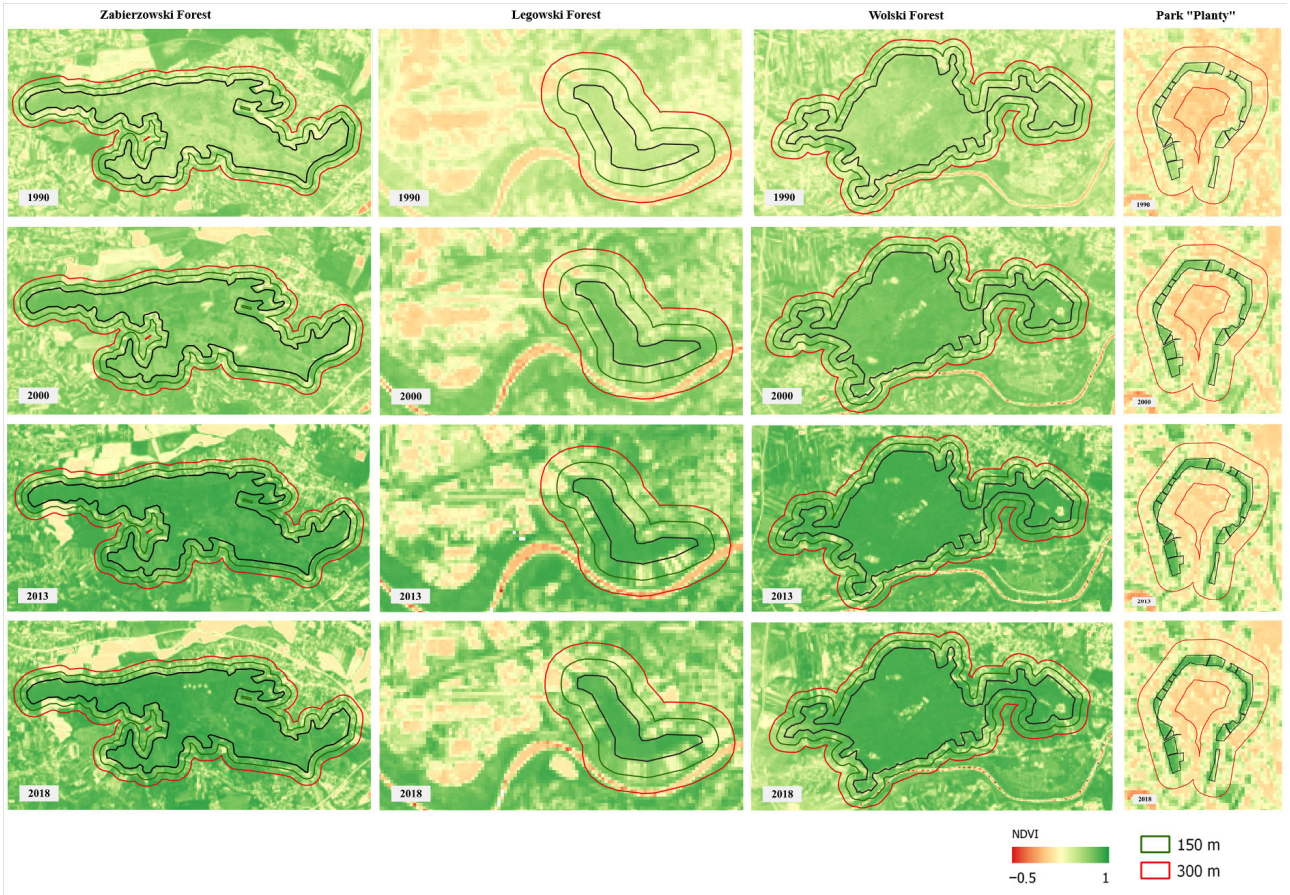

Figure 3. Distributions of NDVI values in the park interiors (0 m) and buffer zones (150 m and 300 m) for the years 1990, 2000, 2013, and 2018. Higher NDVI values (greener areas) are observed inside the parks compared to the urban buffers, and interannual differences reflect varying vegetation conditions (e.g., moisture stress) among the years.

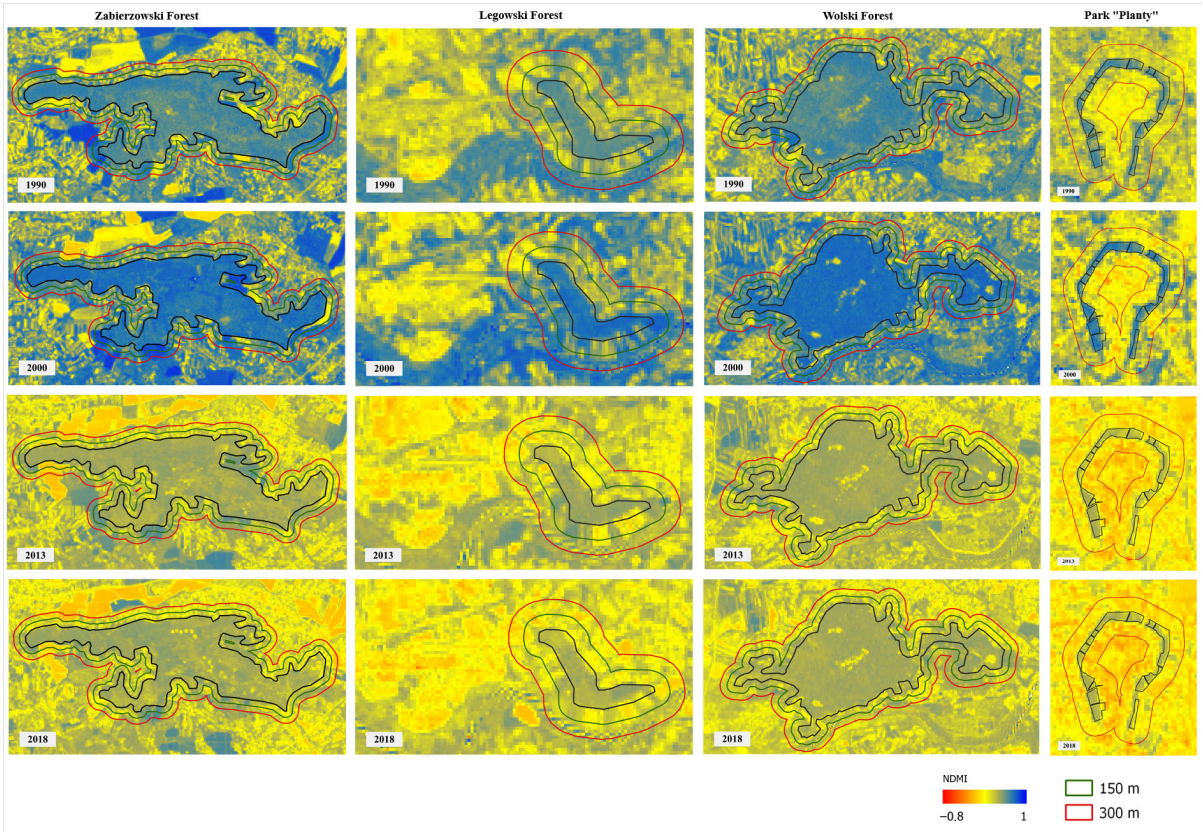

Figure 4. Distributions of NDMI values in the 0 m, 150 m, and 300 m zones for 1990, 2000, 2013, and 2018. NDMI (vegetation moisture index) is highest inside the green areas and decreases with distance into the urban zone. Over time, a slight decline in NDMI can be seen, indicating reduced canopy moisture in later years (particularly 2018, which had lower NDMI inside parks).

3.2. Relationships Between LST and Vegetation (NDVI, NDMI)

The analysis revealed a strong negative correlation between land surface temperature and vegetation indices (NDVI, NDMI) in all four years across all zones. In general, areas with higher greenness or moisture had lower LST. Table 3 summarizes the Pearson correlation coefficients (r) for the LST–NDVI and LST–NDMI relationships in each year. In every year, the park/buffer areas with more vegetation were markedly cooler. Specifically, the LST–NDVI correlation coefficients were r = −0.665 in 1990, −0.944 in 2000, −0.942 in 2013, and −0.915 in 2018. For LST–NDMI, the correlations were: −0.889 (1990), −0.984 (2000), −0.898 (2013), and −0.927 (2018). In 2013, the NDVI correlation ($|r| = 0.942$) slightly exceeded that of NDMI ($|r| = 0.898$), whereas in the other years NDMI's correlation was equal or higher. All these correlations are statistically significant ($p < 0.05$). This means that within each year, zones with lusher (higher NDVI) and especially wetter (higher NDMI) vegetation consistently experienced lower surface temperatures. Overall, NDMI tended to have a slightly stronger association with LST than NDVI, with 2013 as the exception (Table 3), suggesting that vegetation moisture content is a crucial factor in reducing temperatures. The negative relationship indicates that greener and especially wetter areas were markedly cooler than barren or dry areas.

These findings imply that both the amount of vegetation and its moisture status play important roles in modulating urban surface temperatures. NDVI captures the presence and density of plant cover, while NDMI captures the water content in vegetation canopies. The consistently high correlation magnitudes ($|r| \approx 0.9$) show that up to ~80–90% of the spatial variance in LST (within a given year) can be statistically explained by variation in NDVI or NDMI alone. Moreover, the fact that NDMI had a stronger correlation with

LST than NDVI (especially in the peak growing season conditions of 2000) indicates that canopy moisture contributes additional cooling beyond what vegetation amount alone would predict. In practical terms, areas with healthy, well-watered vegetation (high NDMI) were coolest on the land surface.

Table 3. Pearson correlation coefficients between LST and vegetation indices (NDVI and NDMI) for each study year. All correlations are significant at $p < 0.05$.

Year	r(LST, NDVI)	r(LST, NDMI)
1990	−0.665	−0.889
2000	−0.944	−0.984
2013	−0.942	−0.898
2018	−0.915	−0.927

When pooling all the data across years and zones (with appropriate centering to remove annual differences), an overall regression slope of approximately −9 to −11 °C per unit change in the vegetation indices was obtained. Taking into account the relative differences within each year, an increase of 0.1 in NDVI or NDMI was associated with roughly a 0.9–1.1 °C decrease in LST on average. The slope for NDMI was a bit larger in magnitude than that for NDVI, aligning with the year-specific correlations that indicated a greater cooling effect per unit of NDMI. These OLS slopes should not be overinterpreted due to the limited sample size, but they support the notion that enhancing vegetation (especially its moisture content) can yield significant cooling benefits

4. Discussion

4.1. Park Cooling Magnitude and Stability Compared to Other Studies

Across four late-spring, clear-sky epochs (1990, 2000, 2013, 2018), large parks in Kraków were ~2–3 °C cooler than adjacent urban areas (ΔLST between −2.16 and −2.71 °C; Table 2), and this park cool island (PCI) magnitude showed no significant temporal trend over 1990–2018. These outcomes (magnitude and stability) summarize the main findings of this study under seasonally controlled conditions. The observed PCI magnitudes are consistent with results reported for other temperate-climate cities. In Wrocław (Poland), parks were typically 2–3 °C cooler than the built-up fabric [21]. In Nagoya (Japan), large forest parks exhibited ~3–4 °C daytime surface cooling relative to dense urban districts [22]. Meta-analyses synthesizing dozens of sites report mean daytime cooling on the order of ~1 °C with maxima of several degrees depending on context [18,19]. A recent global assessment of >2000 parks across 371 cities found an average daytime cooling of ~1.5 °C, with tree-dominated parks ~3.4 °C cooler than surroundings—placing our ~2–3 °C results toward the upper end expected for large, tree-rich parks in temperate settings [29].

Larger instantaneous differences in LST (up to ~7 °C) have been reported in remote-sensing snapshots of individual parks under hot, dry, clear conditions and specific land-cover configurations [42]. By contrast, our standardized, area-weighted ΔLST provides a conservative city-wide estimate under consistent seasonal and meteorological controls.

Methodological choices help explain variability among studies: (i) the thermal metric (daytime surface temperature vs. near-surface air temperature), (ii) seasonal/meteorological controls, and (iii) spatial context including park size and adjacency [17,18,24]. For example, nocturnal air-temperature cool islands of ~4–6 °C and footprints of ~300 m downwind of large parks have been observed in London [23], whereas our analysis focuses on mid-day surface temperatures and evaluates contrasts within fixed 0–150 m and 150–300 m buffers—scales consistent with typical PCI footprints reported elsewhere [23,26,42].

Within this broader evidence base, Kraków's parks exhibit magnitudes and spatial footprints comparable to those found for large, tree-dominated parks in other temperate cities and—critically—show no measurable attenuation over nearly three decades. This convergence with prior findings strengthens the inference that well-vegetated parks deliver a persistent cooling service under comparable seasonal and meteorological settings.

4.2. Drivers of Park Cooling and Climate Context

Building on Section 4.1, which established a persistent ~2–3 °C PCI, we now quantify the drivers using the study's ΔLST, NDVI/NDMI and spatial gradients. Using the four late-spring, clear-sky epochs, we quantified how vegetation properties relate to land surface temperature (LST). Across all zones and years, LST was strongly and negatively related to both NDVI and NDMI (Table 3). Year-specific correlations for LST–NDMI were −0.889 (1990), −0.984 (2000), −0.898 (2013), −0.927 (2018); for LST–NDVI they were −0.665, −0.944, −0.942, −0.915. In three out of the four years, the magnitude of the NDMI correlation exceeded that of NDVI; the exception was 2013, when NDVI slightly outperformed NDMI (Table 3). In a pooled analysis across all 48 park–zone–year observations, a one-unit increase in NDMI or NDVI was associated with an LST decrease of approximately 9–11 °C (i.e., ~0.9–1.1 °C per 0.1 index), with NDMI exhibiting the larger slope (Section 3.2). Collectively, these quantitative results indicate that vegetation moisture is the dominant proximate driver of the observed cooling, with greenness also contributing.

Spatial gradients around parks reflect the local cooling footprint. The park–urban contrasts were significant in each epoch, with area-weighted ΔLST (park − urban) of −2.16 to −2.36 °C for 0–150 m and −2.31 to −2.71 °C for 150–300 m; all bootstrapped 95% CIs were below 0 °C (Table 2). The similar magnitudes at 0–150 m and 150–300 m imply that cooling remains detectable across at least 300 m from park edges under our measurement conditions. This footprint scale aligns with reports from temperate-climate cities that PCI effects commonly extend a few hundred meters into the urban fabric [23,26,42].

The findings also show that park interiors consistently had higher NDVI and NDMI than adjacent buffers (Figures 3 and 4), and that between 1990 and 2018 NDVI tended to increase slightly while NDMI declined modestly (Table A2). Despite this apparent drying signal, the PCI magnitude remained stable (Sections 3.1 and 3.2), reinforcing that maintaining canopy moisture is critical for sustaining cooling. The mechanistic interpretation is straightforward: shading reduces radiative loading and evapotranspiration removes heat via latent flux [16,17]. Under moisture stress, stomatal closure reduces transpiration and therefore cooling efficiency [27], whereas irrigation or water-sensitive design can enhance evaporative capacity and amplify cooling [28].

From an urban planning perspective, the persistence of a ~2–3 °C daytime park–urban temperature differential in each epoch—despite a ~5–6 °C rise in city-wide LST between 1990 and 2018 (Figure 2; Tables 1 and 2)—indicates that large, tree-dominated green spaces act as reliable long-term heat-mitigation assets. In practical terms, these results support strategies that protect and expand sizeable vegetated parks, ensure continuous canopy cover, and maintain favorable moisture conditions within park boundaries and in the adjacent 0–300 m urban zone where cooling signals remain detectable. Given the consistently strong inverse relationships between LST and vegetation indices—especially NDMI (Table 3)—water availability emerges as a key lever for enhancing cooling; therefore, water-sensitive design and management (e.g., irrigation regimes, soil-moisture conservation, retention features, and species selection resilient to summer drought) can materially increase the effectiveness of park cooling under warming conditions [17,27,28]. Complementary measures in the immediate park surroundings (0–150 m and 150–300 m buffers) include maximizing permeable and vegetated surfaces, strengthening blue–green syner-

gies (e.g., ponds or riparian features where appropriate), and limiting extensive sealed, high-heat-storage materials that erode local cooling benefits [17,24,25]. Taken together, the evidence presented here provides a quantitative basis for prioritizing healthy, moisture-supported urban greenery in climate-adaptation plans and for allocating resources toward the stewardship of park vegetation as a persistent buffer against urban overheating in temperate cities comparable to Kraków. These implications pertain to clear-sky, late-spring daytime conditions analyzed here; other meteorological regimes were beyond the scope of this study.

4.3. Limitations and Future Work

This seasonally controlled, four-epoch analysis is intended as a descriptive baseline; its main limitations concern scope, temporal sampling, metrics, and unobserved covariates. Results derive from four large, tree-dominated green spaces in one city, so inferences are most applicable to similar parks. PCI magnitude and footprint vary with park size, canopy structure, water presence, and surrounding morphology; smaller or isolated greens often show weaker, localized cooling [24–27,42], consistent with ranges synthesized in reviews [18,26]. One clear-sky, late-spring day per epoch provides consistent seasonal snapshots but does not capture inter-annual variability or all-sky conditions. With n = 4 time points, trend tests have low power; consequently, the absence of a detectable trend in ΔLST should be interpreted cautiously (see Section 2.4; Mann–Kendall and related guidance [52,55]). Higher-frequency LST summaries (e.g., annual Landsat composites or daily products) would enable more robust temporal inference. This study analyzed daytime land-surface temperature, which is not identical to 2 m air temperature; magnitudes/footprints are therefore not directly interchangeable, and dedicated in situ micrometeorology or modelling would be required to quantify air-temperature responses [23,26]. Beyond NDVI/NDMI, potentially relevant factors (e.g., soil-water status, irrigation regimes, anthropogenic heat) were not explicitly measured here; a companion mixed-effects analysis begins to address attribution by conditioning on vegetation and year [58]

5. Conclusions

Large urban green spaces in Krakow have provided a consistent cooling benefit over the past three decades, despite significant background warming. From 1990 to 2018, park interiors were on average about 2–3 °C cooler than the surrounding built-up areas in late spring/summer daytime. This park cool island intensity showed no sign of diminishing over time—a trend slope of only +0.007 °C/yr (essentially zero) indicates that the cooling gap between parks and the city remained stable. Meanwhile, the city's overall LST rose by ~5–6 °C, so parks effectively kept pace and continued to offset urban heating each year. It was also observed subtle vegetation changes: NDVI (greenness) in park interiors trended upward slightly, and NDMI (vegetation moisture) trended downward (suggesting possible drying), though neither change was statistically significant. The consistently strong inverse relationship between LST and NDVI/NDMI reinforces that vegetation—particularly its moisture status—is critical in regulating surface temperatures. The results clearly show that providing parks with abundant moisture (through irrigation or designing green spaces for retention) and maintaining lower-density green belts around them effectively enhances the cooling effect. Thus, proper water management and spatial planning can significantly increase the resilience of cities to heat waves. Unlike many engineered solutions, trees and green spaces can continue to provide ecosystem services even as the regional climate warms. The methodology presented, which combining Landsat-derived LST with standardized urban buffers and non-parametric trend analysis, can be readily applied to other cities to assess long-term park cooling performance. Such multi-temporal assessments across

different climates will help determine how universal the persistence of park cooling is, and guide urban planning. In summary, the study provides empirical evidence that investing in healthy, moisture-rich urban green infrastructure yields lasting thermal benefits for cities.

Author Contributions: Author Contributions: Conceptualization, E.G.; methodology, E.G.; software, E.G. and M.K.; validation, E.G.; formal analysis, E.G. and M.K.; investigation, E.G. and M.K.; resources, E.G. and M.K.; data curation, E.G. and M.K.; writing—original draft, E.G.; writing—review and editing, E.G. and M.K.; visualization, E.G. and M.K.; supervision, E.G.; project administration, E.G.; funding acquisition, E.G. All authors have read and agreed to the published version of the manuscript.

Funding: Research project partly supported by program, "Excellence initiative—research university" for the AGH University.

Data Availability Statement: All input datasets are publicly available: Landsat Collection 2 Level 2 scenes from USGS EarthExplorer and CORINE Land Cover/Urban Atlas layers from the Copernicus Land Monitoring Service. The Google Earth Engine and R scripts used to process the data are available from the corresponding author upon reasonable request.

Conflicts of Interest: The authors declare no conflicts of interest.

Abbreviations

The following abbreviations are used in this manuscript:

CLC	CORINE Land Cover
CI	Confidence Interval
EEA	European Environment Agency
EPSG	Coordinate Reference System identifier (EPSG code)
ETM+	Enhanced Thematic Mapper Plus
GEE	Google Earth Engine
IQR	Interquartile Range
LST	Land Surface Temperature
NDMI	Normalized Difference Moisture Index
NDVI	Normalized Difference Vegetation Index
OLI	Operational Land Imager
OLS	Ordinary Least Squares (regression)
PCI	Park Cool Island
QA_PIXEL	Quality Assessment pixel band (Landsat L2)
Q25	25th percentile
Q75	75th percentile
QGIS	Quantum GIS
SC	Single-Channel (LST retrieval)
SD	Standard Deviation
SUHI	Surface Urban Heat Island
Ta	Air temperature
TIRS	Thermal Infrared Sensor
TM	Thematic Mapper
UA	Urban Atlas
UHI	Urban Heat Island
UTC	Coordinated Universal Time
UTM	Universal Transverse Mercator
USGS	United States Geological Survey
WGS 84	World Geodetic System 1984
WRS-2	Worldwide Reference System-2 (Landsat path/row)
ΔLST	Park–urban LST difference (LST_park − LST_urban)

Appendix A

Table A1. Landsat scenes used in the analysis (Kraków area).

Satellite	WRS-2 Path/Row	Date (yyyy-mm-dd)	UTC time (hh:mm:ss)	Scene ID (LANSAT_ID)
Landsat 5	188/25	1990-05-04	08:52:35	LT05_188025_19900504
Landsat 5	188/25	2000-05-15	09:08:13	LT05_188025_20000515
Landsat 8	188/25	2013-05-19	09:34:27	LC08_188025_20130519
Landsat 8	188/25	2018-05-01	09:31:37	LC08_188025_20180501

Table A2. Descriptive statistics (Mean, SD, Q25, Q75, IQR, min–max, n) for LST/NDVI/NDMI in 0 m/150 m/300 m zones, years 1990–2018 (Kraków). n = 4 parks per year.

Variable	Year	Zone	Mean	SD	Q25	Q75	IQR	Min	Max	n
LST	1990	0 m	17.547	0.155	17.457	17.615	0.158	17.387	17.750	4.000
LST	1990	150 m	19.705	0.379	19.565	19.869	0.304	19.220	20.140	4.000
LST	1990	300 m	19.852	0.450	19.690	19.987	0.297	19.330	20.430	4.000
LST	2000	0 m	20.306	0.334	20.198	20.508	0.309	19.833	20.590	4.000
LST	2000	150 m	22.664	0.583	22.511	22.870	0.359	21.900	23.320	4.000
LST	2000	300 m	23.020	0.640	22.854	23.285	0.431	22.150	23.690	4.000
LST	2013	0 m	22.102	0.214	22.012	22.245	0.233	21.810	22.290	4.000
LST	2013	150 m	23.997	0.531	23.788	24.325	0.537	23.270	24.490	4.000
LST	2013	300 m	24.280	0.757	23.918	24.787	0.870	23.280	24.990	4.000
LST	2018	0 m	22.987	0.449	22.730	23.113	0.383	22.610	23.630	4.000
LST	2018	150 m	25.073	0.786	24.593	25.365	0.773	24.360	26.160	4.000
LST	2018	300 m	25.578	0.949	24.908	26.180	1.272	24.600	26.690	4.000
NDMI	1990	0 m	0.592	0.027	0.575	0.600	0.025	0.570	0.630	4.000
NDMI	1990	150 m	0.451	0.069	0.413	0.468	0.054	0.393	0.550	4.000
NDMI	1990	300 m	0.450	0.055	0.417	0.463	0.045	0.409	0.530	4.000
NDMI	2000	0 m	0.700	0.018	0.688	0.712	0.024	0.680	0.720	4.000
NDMI	2000	150 m	0.561	0.046	0.537	0.583	0.046	0.510	0.620	4.000
NDMI	2000	300 m	0.534	0.045	0.513	0.540	0.027	0.500	0.600	4.000
NDMI	2013	0 m	0.405	0.024	0.388	0.422	0.035	0.380	0.430	4.000
NDMI	2013	150 m	0.330	0.042	0.310	0.350	0.040	0.280	0.380	4.000
NDMI	2013	300 m	0.318	0.061	0.280	0.353	0.073	0.250	0.390	4.000
NDMI	2018	0 m	0.402	0.028	0.385	0.422	0.037	0.370	0.430	4.000
NDMI	2018	150 m	0.300	0.018	0.287	0.312	0.025	0.280	0.320	4.000
NDMI	2018	300 m	0.283	0.039	0.255	0.312	0.057	0.240	0.320	4.000
NDVI	1990	0 m	0.569	0.035	0.553	0.575	0.022	0.540	0.620	4.000
NDVI	1990	150 m	0.516	0.052	0.486	0.530	0.044	0.472	0.590	4.000
NDVI	1990	300 m	0.520	0.041	0.497	0.527	0.030	0.489	0.580	4.000
NDVI	2000	0 m	0.712	0.030	0.695	0.726	0.031	0.680	0.750	4.000
NDVI	2000	150 m	0.626	0.034	0.614	0.645	0.031	0.580	0.660	4.000
NDVI	2000	300 m	0.608	0.030	0.595	0.613	0.018	0.580	0.650	4.000
NDVI	2013	0 m	0.858	0.022	0.845	0.873	0.028	0.830	0.880	4.000
NDVI	2013	150 m	0.745	0.034	0.730	0.765	0.035	0.700	0.780	4.000
NDVI	2013	300 m	0.725	0.050	0.705	0.750	0.045	0.660	0.780	4.000
NDVI	2018	0 m	0.870	0.022	0.857	0.877	0.020	0.850	0.900	4.000
NDVI	2018	150 m	0.742	0.030	0.725	0.758	0.033	0.710	0.780	4.000
NDVI	2018	300 m	0.713	0.043	0.690	0.738	0.048	0.660	0.760	4.000

References

1. Nazarian, N.; Krayenhoff, E.S.; Bechtel, B.; Hondula, D.M. Integrated Assessment of Urban Overheating Impacts on Human Life. *Earths Future* **2022**, *10*, e2022EF002706. [CrossRef]
2. Oke, T.R.; Mills, G.; Christen, A.; Voogt, J.A. *Urban Climates*; Cambridge University Press: Cambridge, UK, 2017; ISBN 9781107429536.
3. Imhoff, M.L.; Zhang, P.; Wolfe, R.E.; Bounoua, L. Remote Sensing of the Urban Heat Island Effect Across Biomes in the Continental USA. *Remote Sens. Environ.* **2010**, *114*, 504–513. [CrossRef]
4. Peng, S.; Piao, S.; Lee, X. Surface Urban Heat Island across 419 Global Big Cities. *Environ. Sci. Technol.* **2012**, *46*, 696–703. [CrossRef]
5. Zhou, D.; Zhao, S.; Zhang, L.; Sun, G.; Liu, Y. Remote Sensing of Surface Urban Heat Islands: Progress, Challenges, and Perspectives. *Remote Sens.* **2019**, *11*, 48. [CrossRef]
6. Clinton, N.; Gong, P. MODIS-Detected Surface Urban Heat Islands and Sinks: Global Locations and Controls. *Remote Sens. Environ.* **2013**, *134*, 294–304. [CrossRef]
7. Roy, D.P.; Wulder, M.A.; Loveland, T.R. Characterization of Landsat-7 to Landsat-8 Reflective Wavelength and Radiometric Continuity. *Remote Sens. Environ.* **2016**, *185*, 57–70. [CrossRef]
8. Claverie, M.; Vermote, E.F.; Franch, B.; Masek, J.G. Evaluation of the Landsat-5 TM and Landsat-7 ETM+ Surface Reflectance Products. *Remote Sens. Environ.* **2015**, *169*, 390–403. [CrossRef]
9. Vermote, E.F.; Justice, C.; Claverie, M.; Franch, B. Preliminary Analysis of the Performance of the Landsat 8/OLI Land Surface Reflectance Product. *Remote Sens. Environ.* **2016**, *185*, 46–56. [CrossRef]
10. Jiménez-Muñoz, J.C.; Sobrino, J.A. A Generalized Single-Channel Method for Retrieving Land Surface Temperature from Remote Sensing Data. *J. Geophys. Res. Atmos.* **2003**, *108*, 4688. [CrossRef]
11. Ng, E.; Ren, C. China's Adaptation to Climate and Urban Climatic Changes: A Critical Review. *Urban Clim.* **2018**, *23*, 352–372. [CrossRef]
12. Wang, L.; Lu, Y.; Yao, Y. Comparison of Three Algorithms for the Retrieval of Land Surface Temperature from Landsat 8 Images. *Sensors* **2019**, *19*, 5049. [CrossRef]
13. Almeida, C.R.; Silva, T.; Rodrigues, C. Study of the UHI Using Remote Sensing and LST: A Systematic Review. *Environments* **2021**, *8*, 105. [CrossRef]
14. Lauwaet, D.; Berckmans, J.; Hooyberghs, H.; Wouters, H.; Driesen, G.; Lefebre, F.; De Ridder, K. High-Resolution Modelling of the Urban Heat Island of 100 European Cities (2008–2017). *Urban Clim.* **2024**, *54*, 101850. [CrossRef]
15. Spencer, R.W.; Christy, J.R.; Braswell, W.D. Urban Heat Island Effects in U.S. Summer Surface Temperature Data, 1895–2023. *J. Appl. Meteorol. Clim.* **2025**, *64*, 717–728. [CrossRef]
16. Givoni, B. Impact of Planted Areas on Urban Environmental Quality: A Review. *Atmos. Environ. Part B* **1991**, *25*, 289–299. [CrossRef]
17. Gunawardena, K.R.; Wells, M.J.; Kershaw, T. Utilising Green and Blue Space to Mitigate Urban Heat Island Intensity. *Sci. Total Environ.* **2017**, *584–585*, 1040–1055. [CrossRef]
18. Bowler, D.E.; Buyung-Ali, L.; Knight, T.M.; Pullin, A.S. Urban Greening to Cool Towns and Cities: A Systematic Review of the Empirical Evidence. *Landsc. Urban Plan.* **2010**, *97*, 147–155. [CrossRef]
19. Aram, F.; Higueras García, E.; Solgi, E.; Mansournia, S. Urban Green Space Cooling Effect in Cities. *Heliyon* **2019**, *5*, e01339. [CrossRef]
20. Xie, Q.; Li, J. Detecting the Cool Island Effect of Urban Parks in Wuhan: A City on Rivers. *Int. J. Environ. Res. Public Health* **2021**, *18*, 132. [CrossRef]
21. Blachowski, J.; Hajnrych, M. Assessing the Cooling Effect of Four Urban Parks of Different Sizes in a Temperate Continental Climate Zone: Wroclaw (Poland). *Forests* **2021**, *12*, 1136. [CrossRef]
22. Hamada, S.; Ohta, T. Seasonal Variations in the Cooling Effect of Urban Green Areas on Surrounding Urban Areas. *Urban For. Urban Green.* **2010**, *9*, 15–24. [CrossRef]
23. Doick, K.J.; Peace, A.; Hutchings, T.R. One Large Greenspace Mitigating London's Nocturnal Urban Heat Island. *Sci. Total Environ.* **2014**, *493*, 662–671. [CrossRef]
24. Jaganmohan, M.; Knapp, S.; Buchmann, C.; Schwarz, N. The Influence of Urban Green Space Design on Cooling Effects for Residential Areas. *J. Environ. Qual.* **2016**, *45*, 134–145. [CrossRef]
25. García-Haro, A.; Arellano, B.; Roca, J. Design and Location Influence on Park Cool Island of the Urban Parks of Barcelona. *J. Appl. Remote Sens.* **2023**, *17*, 034512. [CrossRef]
26. Ogce, S.; Ogce, H.; Yu, S.; Brown, R.D. The Interaction between Urban Heat Island and Urban Parks: An In-Situ Measurement-Based Review. *Land Use Policy* **2025**, *157*, 107628. [CrossRef]

27. Kraemer, R.; Kabisch, N. Parks Under Stress: Air Temperature Regulation of Urban Green Spaces Under Conditions of Drought and Summer Heat. *Front. Environ. Sci.* **2022**, *10*, 849965. [CrossRef]
28. Cheung, P.K.; Livesley, S.J.; Nice, K.A. Estimating the Cooling Potential of Irrigating Green Spaces in 100 Global Cities with Arid, Temperate or Continental Climates. *Sustain. Cities Soc.* **2021**, *71*, 102974. [CrossRef]
29. Agathangelidis, I.; Blougouras, G.; Cartalis, C.; Polydoros, A.; Tzanis, C.G.; Philippopoulos, K. Global Climatology of the Daytime Surface Cooling of Urban Parks Using Satellite Observations. *Geophys. Res. Lett.* **2025**, *52*, e2024GL112887. [CrossRef]
30. Matuszko, A.; Mikołajczyk, D.; Matuszko, D. Zmiany Klimatu Krakowa i Adaptacja Do Nich w Kontekście Uwarunkowań Planistycznych. *Pr. Geogr.* **2023**, *170*, 99–118. [CrossRef]
31. Tomczyk, A.M.; Bednorz, E. Thermal Stress During Heat Waves and Cold Spells in Poland. *Weather. Clim. Extrem.* **2023**, *42*, 100612. [CrossRef]
32. Krakowska, M. *Raport o Stanie Metropolii Krakowskiej Za 2023 Rok*; Stowarzyszenie Metropolia Krakowska: Kraków, Poland, 2024.
33. Krzyżewska, A.; Wereski, S.; Dobek, M. Summer UTCI Variability in Poland in the Twenty-First Century. *Int. J. Biometeorol.* **2021**, *65*, 1497–1513. [CrossRef]
34. Las Wolski (Wolski Forest)—Official City Tourism Portal. 2025. Available online: https://krakow.travel (accessed on 30 July 2025).
35. Zabierzów, G. Las Zabierzowski—Walory Krajobrazowe (Official Municipal Page). 2024. Available online: https://zabierzow.org.pl (accessed on 30 July 2025).
36. Krakow City Office. Poznaj Planty—Official City Page (Planty Park). 2019. Available online: https://www.krakow.pl (accessed on 30 July 2025).
37. Krakow City Office. *Program Ochrony Przyrody w Krakowie Na Lata 2019–2030 (Aneks II: Ochrona Przyrody)*; Biuletyn Informacji Publicznej: Warsaw, Poland, 2019. Available online: https://www.krakow.pl (accessed on 30 July 2025).
38. European Environment Agency. *CORINE Land Cover—Nomenclature Guidelines (Level-3 Classes)*; European Environment Agency: Copenhagen, Denmark, 2018.
39. European Environment Agency. *CORINE Land Cover 2018—Technical Guidelines*; European Environment Agency: Copenhagen, Denmark, 2018.
40. Copernicus. Urban Atlas 2018. Copernicus Land Monitoring Service. 2021. Available online: https://land.copernicus.eu/en/products/urban-atlas/urban-atlas-2018 (accessed on 1 May 2025).
41. CLM Service. *Urban Atlas: Vector Land Cover Data*; European Environment Agency: Copenhagen, Denmark, 2018.
42. Du, H.; Cai, W.; Xu, Y.; Wang, Z.; Wang, Y.; Cai, Y. Quantifying the Cool Island Effects of Urban Green Spaces Using Remote Sensing Data. *Urban For. Urban Green.* **2017**, *27*, 24–31. [CrossRef]
43. Tucker, C.J. Red and Photographic Infrared Linear Combinations for Monitoring Vegetation. *Remote Sens. Environ.* **1979**, *8*, 127–150. [CrossRef]
44. Gao, B.-C. NDWI—A Normalized Difference Water Index for Remote Sensing of Vegetation Liquid Water from Space. *Remote Sens. Environ.* **1996**, *58*, 257–266. [CrossRef]
45. Qin, Z.; Karnieli, A.; Berliner, P. A Mono-Window Algorithm for Retrieving Land Surface Temperature from Landsat TM Data and Its Application to the Israel–Egypt Border Region. *Int. J. Remote Sens.* **2001**, *22*, 3719–3746. [CrossRef]
46. Jiménez-Muñoz, J.C.; Cristóbal, J.; Sobrino, J.A.; Soria, G.; Ninyerola, M.; Pons, X. Revision of the Single-Channel Algorithm for Land Surface Temperature Retrieval from Landsat Thermal-Infrared Data. *IEEE Trans. Geosci. Remote Sens.* **2009**, *47*, 339–349. [CrossRef]
47. Carlson, T.N.; Ripley, D.A. On the Relation between NDVI, Fractional Vegetation Cover, and Leaf Area Index. *Remote Sens. Environ.* **1997**, *62*, 241–252. [CrossRef]
48. Sobrino, J.A.; Jiménez-Muñoz, J.C.; Paolini, L. Land Surface Temperature Retrieval from Landsat TM5. *Remote Sens. Environ.* **2004**, *90*, 434–440. [CrossRef]
49. Geological Survey (USGS). *USGS Landsat 8–9 Collection 2 Level-2 Surface Temperature (ST) Product Guide*; Geological Survey (USGS): Reston, VA, USA, 2021.
50. Geological Survey (USGS). *USGS Landsat 4–7 Collection 2 Level-2 Science Products Guide*; Geological Survey (USGS): Reston, VA, USA, 2021.
51. Ermida, S.L.; Soares, P.; Mantas, V.; Göttsche, F.M.; Trigo, I.F. Google Earth Engine Open-Source Code for Land Surface Temperature Estimation from the Landsat Series. *Remote Sens.* **2020**, *12*, 1471. [CrossRef]
52. Mann, H.B. Nonparametric Tests Against Trend. *Econometrica* **1945**, *13*, 245–259. [CrossRef]
53. Sen, P.K. Estimates of the Regression Coefficient Based on Kendall's Tau. *J. Am. Stat. Assoc.* **1968**, *63*, 1379–1389. [CrossRef]
54. Kendall, M.G. *Rank Correlation Methods*; Charles Griffin: London, UK, 1975.
55. Hamed, K.H.; Rao, A.R. A Modified Mann–Kendall Trend Test for Autocorrelated Data. *J. Hydrol.* **1998**, *204*, 182–196. [CrossRef]
56. Seber, G.A.F.; Lee, A.J. *Linear Regression Analysis*, 2nd ed.; Wiley: Hoboken, NJ, USA, 2012; ISBN 9780470436848.

57. Rodgers, J.L.; Nicewander, W.A. Thirteen Ways to Look at the Correlation Coefficient. *Am. Stat.* **1988**, *42*, 59–66. [CrossRef]
58. Głowienka, E.; Kucza, M. Urban Park Vegetation Indices (NDVI, NDMI) and Local Cooling in Krakow: A Linear Mixed-Effects Model Analysis of Landsat LST. *IEEE J. Sel. Top. Appl. Earth Obs. Remote Sens.* 2025; *submitted*.

Disclaimer/Publisher's Note: The statements, opinions and data contained in all publications are solely those of the individual author(s) and contributor(s) and not of MDPI and/or the editor(s). MDPI and/or the editor(s) disclaim responsibility for any injury to people or property resulting from any ideas, methods, instructions or products referred to in the content.